Fluids by design using chaotic surface waves to create a metafluid that is Newtonian, thermal, and entirely tunable

Kyle J. Welch[a,b,1,2], Alexander Liebman-Peláez[a,b,1], and Eric I. Corwin[a,b]

[a]Materials Science Institute, University of Oregon, Eugene, OR 97403; and [b]Department of Physics, University of Oregon, Eugene, OR 97403

Edited by David A. Weitz, Harvard University, Cambridge, MA, and approved July 26, 2016 (received for review April 22, 2016)

In conventional fluids, viscosity depends on temperature according to a strict relationship. To change this relationship, one must change the molecular nature of the fluid. Here, we create a metafluid whose properties are derived not from the properties of molecules but rather from chaotic waves excited on the surface of vertically agitated water. By making direct rheological measurements of the flow properties of our metafluid, we show that it has independently tunable viscosity and temperature, a quality that no conventional fluid possesses. We go on to show that the metafluid obeys the Einstein relation, which relates many-body response (viscosity) to single-particle dynamics (diffusion) and is a fundamental result in equilibrium thermal systems. Thus, our metafluid is wholly consistent with equilibrium thermal physics, despite being markedly nonequilibrium. Taken together, our results demonstrate a type of material that retains equilibrium physics while simultaneously allowing for direct programmatic control over material properties.

Faraday waves | metafluid | emergent thermodynamics

Materials science seeks not only to understand but also to control the properties of matter. To do so, one must dynamically change the nature of conventional materials at the molecular scale. Recent work circumvents this problem by rejecting the molecule as the fundamental unit and substituting a macroscopic structural element. This approach has successfully created metamaterials with novel optical (1–3), acoustic (4–6), mechanical (7–9), and fluid properties (10, 11) that would otherwise be impossible. However, this approach comes at a cost: by deriving their properties from macroscopic, nonequilibrium, or anisotropic elements, these materials necessarily abandon the physics of thermal systems. In this work, using a combination of active and passive rheology, we show that macroscopic chaotic surface waves on a vertically agitated fluid form a fully thermal metafluid with dynamically tunable material properties. In contrast to a conventional fluid in which viscosity and temperature are inextricably linked, we show that these quantities are independently tunable in our system. We further demonstrate that by satisfying the barest criteria of isotropy and steady-state chaos [as required by kinetic theory (12, 13)], we have created a system that obeys the Einstein relation (14). Thus, despite being macroscopic and nonequilibrium, the system is well described by equilibrium thermal physics.

The "molecules" of our metafluid are chaotic Faraday waves (15, 16), generated in a water-filled aluminum dish that is vertically oscillated with rms amplitude A_s and at frequency f_s (Fig. 1 *A* and *C*; see *Materials and Methods* for technical details). The waves uniformly cover the surface of the water and experience significant pinning only at the boundary, far from where our measurements are conducted. The chaos and wave density is holistically steady state, although the existence of a particular wave is transient. Thus, "collisions" in our system refer to encounters between a buoyant tracer and the ephemeral excitations of the chaotic wave environment. We have previously shown chaotic Faraday waves to have a well-defined temperature decoupled from the bath temperature by observing the Brownian motion of a tracer particle (17). We found this temperature to be proportional to shaker amplitude.

Results and Discussion

Drag Coefficient. Our rheometer consists of a driving arm that applies a sinusoidally varying torque $\tau(t)$ at a variable frequency to a buoyant test rotor via a magnetic interaction (Fig. 1 *A–C*; see *Materials and Methods* for technical details). We derive the exact form of this torque in *Materials and Methods* and find that it is well approximated as a Hookean interaction between the drive arm and the test rotor with rotational spring constant $k_r \approx 6\times10^{-5}$ Nm (Fig. S1). Sample time series for the drive arm and test rotor positions are given in Fig. 1*D*.

We program the driving arm's position β to oscillate sinusoidally as

$$\beta(t) = \beta_0 \sin(\omega t), \quad [1]$$

where β_0 is the oscillation amplitude and ω is the angular driving frequency. The resulting motion of the test particle is described by the differential equation

$$I\ddot{\theta} = \tau(t) - \zeta_r\dot{\theta}, \quad [2]$$

where θ is the angular position of the test particle and I is the moment of inertia. Treating the rotor as a damped

Significance

The flow properties of conventional fluids are inextricably linked with their molecular composition; to make water flow like wine would require changing water's molecular identity. In this paper, we show that nonequilibrium chaotic waves excited on the surface of a fluid form a "metafluid," so called because its constitutive dynamics are derived not from the properties of molecules but rather the macroscopic waves. Unlike in conventional fluids, the viscosity and temperature of this metafluid are independently tunable. Despite this unconventional property, our system surprisingly satisfies the Einstein relation, a fundamental characteristic of equilibrium thermal systems. Our metafluid naturally emerges as the result of an external input of energy, thus representing a significant advance in the pursuit of programmable matter.

Author contributions: K.J.W. and E.I.C. designed research; K.J.W. and A.L.-P. performed research; K.J.W. and E.I.C. analyzed data; and K.J.W. and E.I.C. wrote the paper.

The authors declare no conflict of interest.

This article is a PNAS Direct Submission.

[1]K.J.W. and A.L.-P. contributed equally to this work.

[2]To whom correspondence should be addressed. Email: kwelch@uoregon.edu.

This article contains supporting information online at www.pnas.org/lookup/suppl/doi:10.1073/pnas.1606461113/-/DCSupplemental.

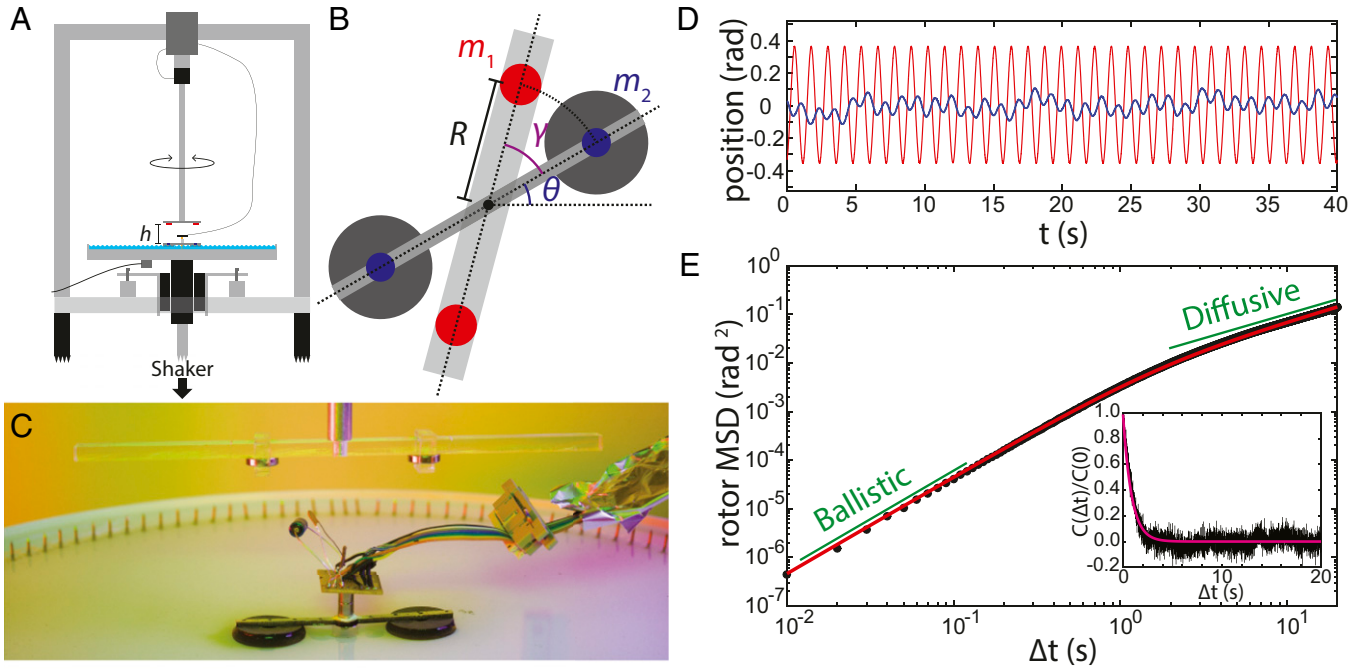

Fig. 1. Experimental setup. (*A*) The rheometer assembly. *h* is the vertical separation of the drive arm and test rotor. (*B*) Top-down cartoon illustrating the coordinates of the system. m_1 and m_2 are the moments of the drive arm and test rotor magnets, respectively; *R* is the radius of rotation of the magnets; θ is the angular position of the test rotor; and γ is the relative angle between the drive arm and test rotor. (*C*) Photograph of the rheometer. (*D*) Example (shaker: $f_s = 60$ Hz, $A_s = 0.064$ mm, drive arm: $\omega/2\pi = 0.8$ Hz) time series of drive arm (red, light) and rotor (blue, dark) positions. (*E*) Example (shaker: $f_s = 60$ Hz, $A_s = 0.064$ mm) MSD. Our data (points) are shown with the prediction for a truly Brownian particle (line) (18, 19). (*E*, *Inset*) Velocity autocorrelation function corresponding to the plotted MSD, with the prediction of the Langevin equation plotted over the data.

driven harmonic oscillator, the solution to this differential equation is

$$\theta(t) = \theta_0 \sin(\omega t + \phi), \quad [3]$$

where the response frequency ω is identical to the driving frequency ω after a brief period as the rotor relaxes into its steady oscillation. All datasets are collected after allowing for this transient period. As derived in *Materials and Methods*, the driving amplitude β_0, oscillation frequency ω, response amplitude θ_0 and phase lag ϕ are related to the drag coefficient ζ_r as

$$\zeta_r = \frac{k_r \beta_0}{\omega \theta_0} \sin\phi. \quad [4]$$

The rotor's response $\theta(t)$ is recorded using a contactless magnetic encoder, and then the response amplitude and phase lag are obtained by using a simple lock-in measurement.

In Fig. 2*A*, we demonstrate that the metafluid behaves as a Newtonian fluid with a drag coefficient that is independent of the rheometer drive frequency over an experimentally relevant range of ω. The above equations also predict (as shown in *Materials and Methods*) a mechanical impedance of

$$Z_m(\omega) = \sqrt{\left(\frac{\zeta_r}{I}\right)^2 + \frac{1}{\omega^2}\left(\frac{k_r}{I} - \omega^2\right)^2}. \quad [5]$$

Fig. 2*B* demonstrates that the measured impedance agrees with the expected form.

Fig. 2*C* shows the results of our active measurement of drag coefficient at values for shaker amplitude and frequency covering the phase space of chaotic Faraday waves. We find that the viscous drag coefficient imparted by the chaotic waves is proportional to the product $A_s f_s$. We can make a heuristic argument to show that this relationship is reasonable. If we hold the shaker amplitude A_s fixed and increase the shaker frequency f_s we will decrease the characteristic wavelength of the surface waves and thus decrease the characteristic time between collisions of the waves and the rotor. If we look to the derivation of the Einstein relation, we see that ζ_r should be inversely proportional to this characteristic time (14) and thus find $\zeta_r \propto f_s$. Likewise, if we hold f_s constant and increase A_s, we will increase the energy in each surface wave, thus increasing the momentum transfer effected by each collision and so increasing the drag coefficient.

The onset of chaos limits our measurement range in shaker amplitude and frequency space, because there exist regions in this space for which the Faraday waves are not chaotic (or, indeed, do not even exist). Nonetheless, we measure the drag coefficient on calm water to be $\zeta_r = 1.9 \times 10^{-5}$ Js, slightly below the lowest drag coefficient that we are able to measure with chaotic waves.

Temperature and Diffusion Constant. To make passive measurements, we remove the driving arm of our rheometer and thus allow the test rotor to diffuse freely while tracking its position. From the position trace, we calculate the mean squared displacement (MSD) $\langle(\Delta\theta)^2\rangle$ and extract two quantities: a mean-squared ballistic angular velocity $\langle\omega_b^2\rangle$ and a rotational diffusion constant D_r. A sample MSD is shown in Fig. 1*E*. Plotted over our data in Fig. 1*E* is the prediction by Ornstein (18) and Fürth (19) for the MSD of a truly Brownian particle. Set into Fig. 1*E* is the velocity autocorrelation corresponding to the plotted MSD, shown with the prediction of the Langevin equation for a thermally diffusing particle. The agreement of predicted thermal behavior with our data demonstrates that our system has the same constituent dynamics as a thermal particle, albeit at much larger length and time scales.

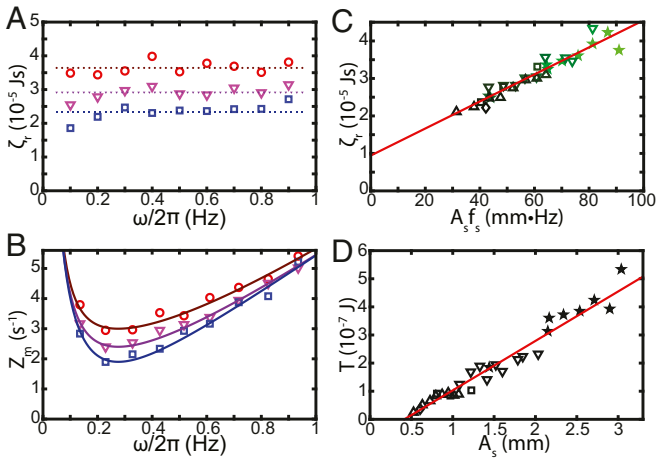

Fig. 2. Tunable Newtonian fluid behavior. (*A*) Demonstration that measured drag coefficient ζ_r is independent of drive arm frequency ω at $A_s = 0.85$ mm and $f_s = 50$ Hz (squares), $A_s = 1.2$ mm and $f_s = 50$ Hz (triangles), and $A_s = 2.4$ mm and $f_s = 30$ Hz (circles). Dotted lines are mean drag coefficient at each amplitude. (*B*) Mechanical impedance Z_m measured at different drive arm frequency ω. Marker shape indicates the same values of A_s and f_s, as in *A*. Solid lines are the expected $Z_m(\omega)$ for a damped driven harmonic oscillator. (*C*) Fitted calibration curve relating rotational drag coefficient to the product of shaker amplitude A_s and shaker frequency f_s. Best fit shown is $\zeta_r \approx (3.6\times10^{-7}$ Js/(mm Hz))$A_s f_s + 9.4\times10^{-6}$Js. Marker color illustrates amplitude; dark-to-light gradient corresponds to low-to-high amplitude variation. Marker shape indicates shaker frequency: $f_s = 30$ Hz (stars), $f_s = 40$ Hz (inverted triangles), $f_s = 50$ Hz (squares), $f_s = 60$ Hz (upright triangles), and $f_s = 70$ Hz (diamonds). (*D*) Fitted calibration curve relating wave temperature T to shaker amplitude A_s. Best fit shown is $T \approx (1.8\times10^{-7}$ J/mm)$A_s - 7.3\times10^{-8}$ J. Marker shape indicates shaker frequency, as in *C*.

For sufficiently small lag times Δt, the MSD appears ballistic: $\langle(\Delta\theta)^2\rangle_{\Delta t_b} = \langle\omega_b^2\rangle\Delta t_b^2$. At longer times, the MSD appears diffusive: $\langle(\Delta\theta)^2\rangle_{\Delta t_d} = 2D_r\Delta t_d$. To avoid the biases associated with the traditional method of fitting the MSD to estimate $\langle\omega_b^2\rangle$ and D_r, we instead choose the smallest lag times Δt_b and Δt_d that are convincingly ballistic and diffusive (20), respectively, and estimate $\langle\omega_b^2\rangle$ and D_r using

$$\langle\omega_b^2\rangle = \frac{\left\langle(\Delta\theta)^2\right\rangle_{\Delta t_b} - \sigma^2}{\Delta t_b^2} \qquad [6]$$

and

$$D_r = \frac{\left\langle(\Delta\theta)^2\right\rangle_{\Delta t_d} - 2\sigma^2}{2\Delta t_d}, \qquad [7]$$

where $\sigma^2 = 3.7\times10^{-5}$ rad^2 is the positional error associated with the discrete nature of the magnetic rotary encoder output. Finally, given the hydrodynamic moment of inertia I_h for the rotor, equipartition gives us the temperature as $T = I_h\langle\omega_b^2\rangle$.

Fig. 2*D* confirms our previous finding that temperature is proportional to shaker amplitude A_s (17). We would expect the temperature of the system to be proportional to the energy density in the surface waves, which is itself proportional to the amplitude squared as $T \propto A_{waves}^2$. We can understand the linear dependence of T on the shaker amplitude A_s by considering the response properties of Faraday waves. In such systems, the characteristic response amplitude is generally proportional to the square root of the driving amplitude (21), so $A_{waves} \propto A_s^{1/2}$, which leads to $T \propto A_s$.

The temperatures we measure here from rotational motion are consistent with the temperature we measured in earlier work on translational motion (17), giving further credence to the notion that our system demonstrates energy equipartition and is truly thermal. The measured temperature is a remarkable 14 orders of magnitude larger than the water bath temperature, demonstrating that the thermal behavior of our system is completely divorced from that of ordinary matter.

Einstein Relation and Hydrodynamic Moment of Inertia. Thermal fluids satisfy the Einstein relation, which states that $D_r\zeta_r = T$. The power of the Einstein relation is that it connects two very different properties of fluids: rheology (a measurement of correlated many-body behavior) and diffusion (a measurement of single-particle dynamics). There is no a priori reason to expect the Einstein relation to hold in a nonequilibrium complex fluid such as ours in which energy is constantly being injected into the system. Nonetheless, Fig. 3*A* demonstrates that the Einstein relation is satisfied. That we discover an intact Einstein relation further convinces us that our macroscopic metafluid is in fact an equilibrium fluid. Additionally, Fig. 3*B* shows that the diffusion constant calculated from the MSD is consistent with the diffusion

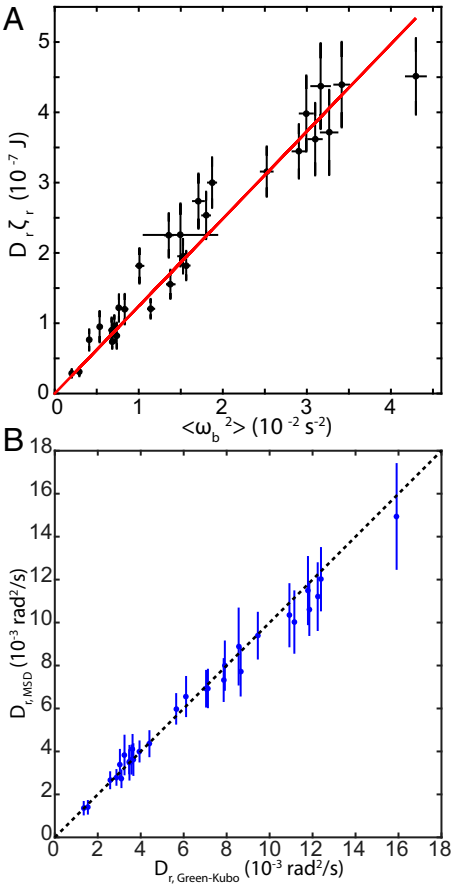

Fig. 3. (*A*) Demonstration of the Einstein relation in our system. The product $D_r\zeta_r$ is proportional to the angular mean square ballistic velocity $\langle\omega_b^2\rangle$, which is, in turn, proportional to the effective temperature of the waves T. The line shown is a fit to the data of the Einstein relation $D_r\zeta_r = I_h\langle\omega_b^2\rangle$, with the hydrodynamic moment of inertia I_h left as a free parameter, determined by the fitting to be $I_h = 1.2\times10^{-5}$ kg m^2. The error bars shown are 1σ confidence intervals determined from the calculation of D_r and $\langle\omega_b^2\rangle$. (*B*) Comparison of diffusion constant measured from MSD ($D_{r,MSD}$) and using the Green–Kubo relations ($D_{r,Green-Kubo}$). The dashed line has slope 1, indicating good agreement between the two methods of calculating D_r.

constant as calculated using the Green–Kubo relations, which relate the diffusion constant to the integral of the velocity autocorrelation function. This consistency convinces us that Einstein relation in our system may be trusted over all timescales available to our measurement. Taken together, these results suggest that the universality of thermal systems should be extended to systems which satisfy broader criteria of steady-state chaos and isotropy.

This notion of universality is supported by work done in other driven, dissipative systems. For example, the work of Ojha et al. (22) demonstrated that a particle agitated by turbulent airflow is identically thermal with a temperature completely divorced from the room temperature. Here, we have used an unconventional mechanism for thermalization and yet, nevertheless, recover thermal behavior, also with a temperature completely divorced from that of the surroundings. Our work further demonstrates that these macroscopic thermal systems can be tuned in ways that microscopic systems cannot.

The slope of the fitted line relating $\langle\omega_b^2\rangle$ and $D_r\zeta_r$ in Fig. 3*A* is the hydrodynamic moment of inertia I_h, as $T = I_h\langle\omega_b^2\rangle$. This quantity is larger than the moment calculated directly from the mass and geometry of the test rotor by nearly an order of magnitude due to the fact that a volume of water is swept along with the rotor.

We have thus far shown that $T \propto A_s$, $\zeta_r \propto A_s f_s$ and $D_r\zeta_r = T$. Taken together, these results imply that $D_r \propto 1/f_s$. We can heuristically understand this relationship by realizing that shaker frequency is inversely related to the characteristic wavelength of the chaotic surface waves. As shaker frequency decreases, the characteristic wavelength increases. Because the average distance between wave excitations is greater, the mean free path and mean free time of a diffusing particle increase proportionally. The diffusion constant is proportional to $(\text{mean free path})^2/(\text{mean free time})$. By this line of reasoning, D_r should be proportional to $1/f_s$.

Our results also imply that D_r should not depend strongly on shaker amplitude A_s. We can understand this relationship heuristically as well. As the shaker amplitude increases, so too does the amplitude of the waves, as we outlined in our discussion of why $T \propto A_s$. This increase in amplitude increases the strength of the kicks that set a particle in motion, but also increase the strength of the kicks that slow it down. The increase in thermal energy is offset by the energy dissipated by the drag coefficient, which also increases with shaker amplitude. Thus, it is reasonable that D_r not depend strongly on A_s.

Tunable Thermal Newtonian Metafluid. We have demonstrated three properties of this metafluid: (*i*) the metafluid has a well-defined Newtonian viscous drag which is controlled by the product of shaker amplitude and frequency; (*ii*) the metafluid has a well-defined temperature, which is controlled by shaker amplitude; and (*iii*) the metafluid satisfies the Einstein relation. These results lead to the inevitable conclusion that our system is in fact a thermal Newtonian metafluid with independently tunable material properties, as shown in Fig. 4. Any arbitrary state or path in $D_r - \zeta_r - T$ space that satisfies the Einstein relation is translatable using our measured calibration curves into the $f_s - A_s$ parameter space. An example $D_r - \zeta_r - T$ path is shown in red in Fig. 4*A* and then shown translated into a corresponding $f_s - A_s$ path in Fig. 4*B* using the Einstein relation and the calibration curves shown in Fig. 2 *C* and *D*.

The surface defined by the Einstein relation is shown as the background gradient in Fig. 4*A*, with color indicating temperature. Each trial measurement of our system is able to sit anywhere along this surface, as shown by the plotted points in Fig. 4*A*. The color of the plotted points indicates the measured temperature for that trial, and we see, as in Fig. 3*A*, that our system agrees with the Einstein relation.

Conventional fluids, by contrast, lack the freedom to move arbitrarily about this surface, because they suffer from the additional constraint that viscous drag is a function of temperature. For example, viscous drag in an ideal gas is related to temperature as $\zeta \propto T^{1/2}$ (and thus $\zeta \propto D_r$), as shown in the representative ideal gas model curve in Fig. 4*A* (dashed line). To change the constant of proportionality, one would need to change the molecular composition of the gas or, put more plainly, one would need to change the very identity of the gas. A conventional fluid is therefore confined to a single curve through $D_r - \zeta_r - T$ space.

In this paper, we have presented a fully tunable, thermal Newtonian metafluid. By combining passive and active rheology, we directly measure diffusion, temperature, and viscous drag in a system of chaotic surface waves and show that they are independently manipulable. The Einstein relation is satisfied even though our system is both macroscopic and nonequilibrium, hinting that a broader universality exists in random systems: so long as steady-state, isotropic chaos exists, the system may be mapped onto an equilibrium statistical mechanical system. This reading of the data is supported by previous studies of thermal behavior in driven, dissipative systems with inherent randomness (22).

We have followed in the footsteps of previous metamaterial research (1–11), creating and characterizing an unconventional material by rejecting the atom as the fundamental thermal unit and substituting a macroscopic element, in our case, with chaotic

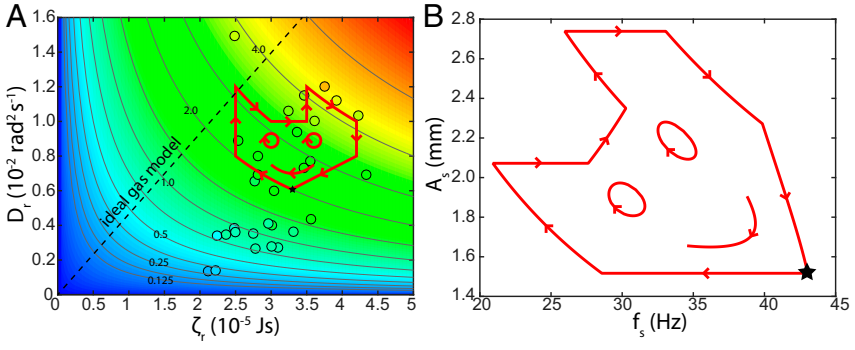

Fig. 4. (*A*) Phase space. Measured diffusion constant plotted against measured drag coefficient (circles). Marker color indicates measured temperature, which is in reasonable agreement with the background gradient that represents temperature as calculated from the Einstein relation, $T = D_r\zeta_r$. Example isotherms (black lines) are shown, labeled in units of 10^{-7} J. Our system can take any path along the surface defined by the Einstein relation, whereas a conventional fluid is confined to a particular curve (ideal gas behavior shown as an example). An example path through $D_r - \zeta_r - T$ phase space beginning at the star is plotted and is then transformed into $f_s - A_s$ parameter space (*B*) via the Einstein relation and the calibration curves shown in Fig. 2 *C* and *D*.

surface waves. Our system provides a platform in which experiments may be performed, where the tools of thermodynamics remain intact and the fluid properties can be controlled in real time. There are obvious limitations, for example, the metafluid cannot flow through a pipe; it cannot be compressed, nor is there an easy way to define pressure; and it is confined to two dimensions. However, we have already shown it to be useful in observing the atomistic dynamics of 2D polymer analogs (23), and we believe that it will prove elucidating in many open questions of the thermal world, such as self-assembly and 2D pattern formation (24–26). Perhaps, emergent metafluids such as ours exist throughout the macroscopic world, be they swarms, turbulent weather, financial markets, or any other system with intrinsic randomness.

Materials and Methods

Shaker Assembly. The waves are generated in a water-filled aluminum dish (diameter, 17.5 inches; depth, 0.5 inches) that is vertically oscillated with rms amplitude A_s and at frequency f_s (Fig. 1*A*). The dish is mounted on a ceramic-coated aluminum shaft (diameter, 2 inches), which passes through a 2-inch inner diameter air bushing (New Way Air Bearings). This assembly is leveled by a stage mounted to the outside of the bushing mounting block. The ceramic-coated shaft is connected by a 24-inch length of 1-inch T-slot framing to an electromechanical shaker (VTS-100; Vibration Test Systems) controlled by a digital function generator (Model DS335; Stanford Research Systems) through a voltage amplifier (Europower EP4000; Behringer). Four springs connect the T-slot framing shaft to the external armature, bearing nearly all of the static load. An accelerometer is mounted to the bottom of the dish to measure stroke amplitude and frequency through a digital oscilloscope (TDS 2012C; Tektronix).

Rheometer. The driving arm of the rheometer is laser-cut from acrylic and has attached to it two neodymium magnets (cylinder magnets; thickness, 0.125 inches; diameter, 0.5 inches; moment $m_1 = 0.42$ A m^2; K&J Magnetics). Each magnet is positioned $R = 3$ cm from the center of the arm with their north poles up. The driving arm sits at the end of a long aluminum shaft and is rotated about its center by a stepper motor driven by an Arduino Uno. The long shaft ensures that there is no effect due to magnetic interactions with the stepper motor. The test rotor consists of two closed-cell nylon foam disk floats held at the same $R = 3$ cm from the center as the driving arm magnets by a laser-cut piece of balsa wood. The wood piece has a hole in its center which, when slipped over a Delrin post set into the center of the dish, holds the test rotor coaxial with the driving arm but free to rotate. In the center of each float disk is a neodymium magnet (cylinder magnets; thickness, 0.0625 inches; diameter, 0.25 inches; moment $m_2 = 0.053$ A m^2; K&J Magnetics) with its north pole up. The vertical separation between the driving arm and the test rotor is $h = 6$ cm. A contactless magnetic encoder (part no. AEAT-6600-T16; Avago Technologies) is used to track the angular position of the test particle. To facilitate tracking, a cylindrical, diametric (polarization orthogonal to the axis of symmetry) magnet with an axial pass-through hole is mounted in the center of the wooden connector. The magnetic encoder is mounted on top of the center post and is recorded by a second Arduino Uno.

Derivation of Torque Due to Magnets. Here, we derive, in exact form, the torque on the test rotor as a function of relative angle γ.

We begin by defining all salient parameters and variables. Fig. 1 *A* and *B* illustrates the relationship between the quantities. θ is the angular position of the test rotor; γ is the relative angle between the drive arm and test rotor when viewed from above; R is the distance of the magnets from the axis of rotation; $\vec{m}_1 = m_1\hat{z}$ and $\vec{m}_2 = m_2\hat{z}$ are the magnetic moments of the upper and lower magnets, respectively; $\vec{r}$ is the separation of the upper magnet from the lower magnet; a is the lateral distance between the upper and lower magnets (defining the $\hat{x}$ direction); and h is the vertical distance between the upper and lower magnets.

The coordinates and dimensions of the system are related to one another as

$$r = \sqrt{h^2 + a^2} = \sqrt{h^2 + 4R^2 \sin^2\left(\frac{\gamma}{2}\right)}. \quad [8]$$

Given that $\vec{m}_1 = m_1\hat{z}$, $\vec{m}_2 = m_2\hat{z}$ and $\vec{r}\cdot\hat{z} = h$, the force between the upper and lower magnets is

$$\vec{F}\left(\vec{r}, \vec{m}_1, \vec{m}_2\right) = \frac{3\mu_o m_1 m_2}{4\pi r^5}\left(2h\hat{z} + \left(1 - \frac{5h^2}{r^2}\right)\vec{r}\right). \quad [9]$$

The exerted in-plane torque is driven by the component of the force that is directed tangent to the arc of rotation. To obtain this force, we first find the $\hat{x}$ component of $\vec{F}$, which lies along a. Noting that $\vec{r}\cdot\hat{x} = a$, we can write the $\hat{x}$ component of $\vec{F}$ as

$$F_x = \vec{F}\cdot\hat{x} = \frac{3\mu_o m_1 m_2 R}{2\pi r^5}\left(1 - \frac{5h^2}{r^2}\right)\sin\left(\frac{\gamma}{2}\right). \quad [10]$$

We calculate the component of the force tangent to the arc of rotation $F_\gamma = F_x\cos\left(\frac{1}{2}\gamma\right)$ and thus the torque $\tau = F_\gamma R$ using the identity $\sin\left(\frac{1}{2}\gamma\right)\cos\left(\frac{1}{2}\gamma\right) = \frac{1}{2}\sin\gamma$ to obtain

$$\tau(\gamma) = \frac{3\mu_o m_1 m_2 R^2}{2\pi}\left(\frac{1}{r^5} - \frac{5h^2}{r^7}\right)\sin\gamma. \quad [11]$$

This equation is the exact form for the torque on the test particle as a function of relative angle γ, with an extra factor of 2 to account for the fact that our system has two pairs of magnets. For simplicity, we would like to approximate this torque as Hookean. To obtain a Hookean form, we make the approximation that $r \approx h$ and $\sin\gamma \approx \gamma$, which is a small-angle approximation and will break down as γ increases. The Hookean torque we obtain is

$$\tau(\gamma) = -k_r\gamma, \quad [12]$$

where

$$k_r = \frac{6\mu_o m_1 m_2 R^2}{\pi h^5}. \quad [13]$$

For the particular parameters of our system, $k_r \approx 6\times10^{-5}$ Nm. Fig. S1 shows the torque in exact form and the linear approximation over a range of relevant angles.

Measurement of Drag Coefficient. We program the driving arm's position β to oscillate sinusoidally as

$$\beta(t) = \beta_0\sin(\omega t), \quad [14]$$

where β_0 is the oscillation amplitude and ω is the angular driving frequency. Assuming a well-defined coefficient of drag, the resulting motion of the test particle is described by the differential equation

$$I\ddot{\theta} = \tau(t) - \zeta_r\dot{\theta}, \quad [15]$$

where θ is the angular position of the test particle, I is the moment of inertia, $\tau(t)$ is the torque applied by the driving arm, and ζ_r is the rotational drag coefficient. The applied torque τ is only dependent on the relative angle $\gamma(t) = \theta(t) - \beta(t)$ between the driving arm and the test particle and so can be parameterized as $\tau(t) = \tau(\gamma(t))$. We derive the exact form of this torque above and find that it is well approximated by a Hookean spring:

$$\tau(\gamma) = -k_r\gamma, \quad [16]$$

with spring constant

$$k_r = \frac{6\mu_0 m_1 m_2 R^2}{\pi h^5} \approx 6\times10^{-5}\ \text{Nm}. \quad [17]$$

Here, m_1 and m_2 are the magnitudes of the magnetic moments of the driving arm and test particle magnets, respectively. This approximation allows us to solve Eq. **15** exactly as a damped driven harmonic oscillator to find

$$\theta(t) = \theta_0\sin(\omega t + \phi), \quad [18]$$

where

$$\theta_0 = \beta_0\frac{k_r}{I\omega Z_m(\omega)}, \quad [19]$$

the mechanical impedance is

$$Z_m(\omega) = \sqrt{\left(\frac{\zeta_r}{I}\right)^2 + \frac{1}{\omega^2}\left(\frac{k_r}{I} - \omega^2\right)^2}, \quad [20]$$

and the phase lag is

PHYSICS

$$\phi(\omega) = \tan^{-1}\left(\frac{\zeta_r}{I}\frac{\omega}{\omega^2 - \frac{k_r}{I}}\right). \quad [21]$$

We solve for the drag coefficient to find

$$\zeta_r = \frac{k_r \beta_0}{\omega \theta_0}\sin\phi. \quad [22]$$

Thus, we are able to calculate the drag coefficient by measuring the amplitude and phase lag of the test rotor's response relative to the driving signal. We obtain the response amplitude and phase lag using a simple lock-in measurement:

$$\theta_0 = \left(\langle\theta(t)\cos(\omega t)\rangle^2 + \langle\theta(t)\sin(\omega t)\rangle^2\right)^{1/2}, \quad [23]$$

$$\phi = \tan^{-1}\left(\frac{\langle\theta(t)\sin(\omega t)\rangle}{\langle\theta(t)\cos(\omega t)\rangle}\right), \quad [24]$$

where the angle brackets indicate time averages.

ACKNOWLEDGMENTS. We thank Raghu Parthasarathy, John Royer, and John Toner for helpful discussions. This work was supported by National Science Foundation (NSF) Career Award DMR-1255370. A.L.-P. was supported under the Research Experience for Undergraduates program, sponsored by the University of Oregon Materials Science Institute and the NSF.

1. Smith DR, Pendry JB, Wiltshire MCK (2004) Metamaterials and negative refractive index. *Science* 305(5685):788–792.
2. Tsakmakidis KL, Boardman AD, Hess O (2007) 'Trapped rainbow' storage of light in metamaterials. *Nature* 450(7168):397–401.
3. Valentine J, et al. (2008) Three-dimensional optical metamaterial with a negative refractive index. *Nature* 455(7211):376–379.
4. Liu Z, et al. (2000) Locally resonant sonic materials. *Science* 289(5485):1734–1736.
5. Brunet T, Leng J, Mondain-Monval O (2013) Materials science. Soft acoustic metamaterials. *Science* 342(6156):323–324.
6. Süsstrunk R, Huber SD (2015) PHYSICS. Observation of phononic helical edge states in a mechanical topological insulator. *Science* 349(6243):47–50.
7. Silverberg JL, et al. (2014) Applied origami. Using origami design principles to fold reprogrammable mechanical metamaterials. *Science* 345(6197):647–650.
8. Waitukaitis S, Menaut R, Chen BG, van Hecke M (2015) Origami multistability: From single vertices to metasheets. *Phys Rev Lett* 114(5):055503.
9. Silverberg JL, et al. (2015) Origami structures with a critical transition to bistability arising from hidden degrees of freedom. *Nat Mater* 14(4):389–393.
10. Rankin PJ, Ginder JM, Klingenberg DJ (1998) Electro- and magneto-rheology. *Curr Opin Colloid Interface Sci* 3(4):373–381.
11. Ozaki R, Aoki M, Yoshino K, Toda K, Moritake H (2010) Effective viscosity for nematic-liquid-crystal viscosity measurement using a shear horizontal wave. *Phys Rev E Stat Nonlin Soft Matter Phys* 81(6 Pt 1):061703.
12. Maxwell JC (1867) On the dynamical theory of gases. *Philos Trans R Soc Lond* 157:49–88.
13. Boltzmann L (1909) *Wissenschaftliche Abhandlungen*, ed Hasenohrl F (Barth, Leipzig, Germany), Vol 1.
14. Einstein A (1905) Über die von der molekularkinetischen Theorie der Wärme geforderte Bewegung von in ruhenden Flüssigkeiten suspendierten Teilchen [On the movement of small particles suspended in a stationary liquid demanded by the molecular-kinetic theory of heat]. *Ann Phys* 322(8):549–560. German.
15. Faraday M (1831) On a peculiar class of acoustical figures; and on certain forms assumed by a group of particles upon vibrating elastic surfaces. *Philos Trans R Soc Lond* 121:299–340.
16. Rayleigh L (1883) On the crispations of fluid resting upon a vibrating support. *Philos Mag* 16(5):50–58.
17. Welch KJ, Hastings-Hauss I, Parthasarathy R, Corwin EI (2014) Ballistic and diffusive dynamics in a two-dimensional ideal gas of macroscopic chaotic Faraday waves. *Phys Rev E Stat Nonlin Soft Matter Phys* 89(4):042143.
18. Ornstein LS (1919) On the Brownian motion. *Proc Acad Amst* 21:96–108.
19. Fürth R (1920) Die Brownsche Bewegung bei Berücksichtigung einer Persistenz der Bewegungsrichtung. *Z Physik* 2:244–256. German.
20. Vestergaard CL, Blainey PC, Flyvbjerg H (2014) Optimal estimation of diffusion coefficients from single-particle trajectories. *Phys Rev E Stat Nonlin Soft Matter Phys* 89(2):022726.
21. Wernet A, Wagner C, Papathanassiou D, Müller HW, Knorr K (2001) Amplitude measurements of Faraday waves. *Phys Rev E Stat Nonlin Soft Matter Phys* 63(3 Pt 2): 036305.
22. Ojha RP, Lemieux PA, Dixon PK, Liu AJ, Durian DJ (2004) Statistical mechanics of a gas-fluidized particle. *Nature* 427(6974):521–523.
23. Welch KJ, Kilmer CSG, Corwin EI (2015) Atomistic study of macroscopic analogs to short-chain molecules. *Phys Rev E Stat Nonlin Soft Matter Phys* 91(2):022603.
24. Whitesides GM, Grzybowski B (2002) Self-assembly at all scales. *Science* 295(5564): 2418–2421.
25. Tricard S, et al. (2012) Analog modeling of Worm-Like Chain molecules using macroscopic beads-on-a-string. *Phys Chem Chem Phys* 14(25):9041–9046.
26. Cademartiri R, et al. (2012) A simple two-dimensional model system to study electrostatic-self-assembly. *Soft Matter* 8(38):9771–9791.

Supporting Information

Welch et al. 10.1073/pnas.1606461113

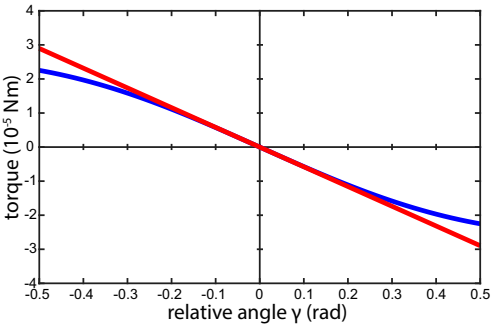

Fig. S1. Comparison of Hookean approximation and full form for torque exerted by drive arm. The full form torque (blue) is well approximated by a Hookean torque with spring constant $k_r \sim 6 \times 10^{-5}$ Nm (red) over a range of angles relevant to our active measurement of drag coefficient.